



Loss of odor-induced c-Fos expression of juxtglomerular activity following maintenance of mice on fatty diets

Erminia Fardone^{1,2,3} · Arda B. Celen^{1,4} · Nicholas A. Schreiter^{1,5} · Nicolas Thiebaud^{1,2} · Melissa L. Cooper^{1,6} · Debra Ann Fadool^{1,2,7}

Received: 1 June 2018 / Accepted: 27 August 2018 / Published online: 11 September 2018
© Springer Science+Business Media, LLC, part of Springer Nature 2018

Abstract

Diet-induced obesity (DIO) decreases the number of OMP+ olfactory sensory neurons (OSN) in the olfactory epithelium by 25% and reduces correlate axonal projections to the olfactory bulb (OB). Whether surviving OSNs have equivalent odor responsivity is largely unknown. Herein, we utilized *c-fos* immediate-early gene expression to map neuronal activity and determine whether mice weaned to control (CF), moderately-high fat (MHF), or high-fat (HF) diet for a period of 6 months had changes in odor activation. Diet-challenged *M72-IRE5-tau-GFP* mice were exposed to either a preferred M72 (Olf160) ligand, isopropyl tiglate, or clean air in a custom-made Bell-jar infusion chamber using an alternating odor exposure pattern generated by a picospritzer™. Mice maintained on fatty diets weighed significantly more and cleared glucose less efficiently as determined by an intraperitoneal glucose tolerance test (IPGTT). The number of juxtglomerular cells (JGs) decreased following maintenance of the mice on the MHF diet for cells surrounding the medial but not lateral M72 glomerulus within a 4 cell-column distance. The percentage of *c-fos* + JGs surrounding the lateral M72 glomerulus decreased in fat-challenged mice whereas those surrounding the medial glomerulus were not affected by diet. Altogether, these results show an asymmetry in the responsiveness of the ‘mirror image’ glomerular map for the M72 receptor that shows greater sensitivity of the lateral vs. medial glomerulus upon exposure to fatty diet.

Keywords Olfactory bulb · Diet-induced obesity · Olfactory · M72 · Olf160 · Obesity

Introduction

The incidence of diet-induced obesity (DIO) has risen across the globe in the past thirty years (Moyer 2012; Ogden et al. 2014) and is attributed to lack of exercise and poor diet. It is one of the main contributors to preventable diseases worldwide. Currently in the United States, 30% of the population is

considered obese with a body mass index (BMI) greater than 30 kg/m² and 1 in 20 individuals are morbidly obese (BMI > 40 kg/m²) (Ogden et al. 2014). All organ systems of the body are affected by DIO, including the brain and peripheral nervous system, which are particularly vulnerable to metabolic dysfunction. Changes in brain volume and cognition can occur in response to brain injury induced by obesity (Bruce-

✉ Debra Ann Fadool
dfadool@bio.fsu.edu

Erminia Fardone
erminia.fardone@live.com

Nicholas A. Schreiter
nschreiter@wisc.edu

Melissa L. Cooper
melissa.cooper@vanderbilt.edu

¹ Department of Biological Science, The Florida State University, KIN Life Science Building, 319 Stadium Drive, Suite 3014, Tallahassee, FL 32306, USA

² Program in Neuroscience, The Florida State University, 319 Stadium Drive, Suite 3014, Tallahassee, FL 32306, USA

³ Present address: Histology and Anatomy Shared Resource, HHMI Janelia Research Campus, 19700 Helix Drive, Ashburn, VA 20147, USA

⁴ Present address: Boğaziçi University - Molecular Biology and Genetics, 34342 Bebek, 34730 Istanbul, Turkey

⁵ Present address: School of Medicine and Public Health, University of Wisconsin-Madison, 750 Highland Avenue, Madison, WI 53726, USA

⁶ Present address: Vanderbilt Eye Institute, 11425 Langford MRBIV, 2213 Garland Avenue, Nashville, TN 37232, USA

⁷ Institute of Molecular Biophysics, The Florida State University, 319 Stadium Drive, Suite 3014, Tallahassee, FL 32306, USA

Keller et al. 2009). The operation of our sensory systems thereby, is also affected by metabolic state, energy imbalance, or disruption of endocrine hormones that commonly accompany DIO (Fadool et al. 2011; Tucker et al. 2012; Ogden et al. 2014; Thiebaud et al. 2014). Olfaction is one of the major modalities that contributes to hedonic evaluation of food, resulting in food choice and possible consumption (Yeomans 2006). It is not surprising that changes in olfactory function incurred by energy imbalance may act as a positive feedback loop to drive further dysregulation of olfactory perception in individuals with DIO (Palouzier-Paulignan et al. 2012; Tucker et al. 2012; Thiebaud et al. 2014).

We have previously demonstrated that mice made obese through maintenance on modified fatty diets had reduced olfactory perception, poor olfactory learning, diminished neuronal excitability of the olfactory bulb, and lesser survival of olfactory sensory neurons (OSNs) and their concomitant axonal projections (Fadool et al. 2011; Tucker et al. 2013; Thiebaud et al. 2014). While mice with DIO are not anosmic, they do exhibit failed detection of certain food odorants (Tucker et al. 2013) and have a reduced electroolfactogram (EOG) amplitude in response to an odorant dose-response curve (Thiebaud et al. 2014). The loss of EOG amplitude implicated a reduced contribution from M72-expressing OSNs, which were histologically examined to be markedly reduced in mice maintained on either a moderately-high (32% fat) or high-fat (60%) chow diet (Thiebaud et al. 2014). A reduction in olfactory marker protein positive (OMP+) neurons as well as a reduced expression of G protein olfactory (G_{olf}) and another odorant receptor, MOR28 (Olf1507), implicated a loss of OSNs beyond that of M72 (Olf160). There was a 25% loss of OSNs throughout the endoturbinates IIB, however, the specifics of how DIO might differentially impact OR classes or defined glomeruli is unknown.

DIO causes a loss of OSNs but a more refined understanding of the functionality of the surviving neurons or the mechanism regulating the loss of DIO-sensitive neurons has not been explored. Interestingly, we observed that DIO induces OSN apoptosis yet simultaneously enhances basal cell proliferation in the main olfactory epithelium (MOE) with accompanying microglial inflammation (Thiebaud et al. 2014). Mice maintained on a fatty diet for six months that have a reduced ability to clear glucose have a reduced ability to discriminate simple odorant pairs in a go no-go operant conditioning paradigm and have a complete inability to reversal learn (Thiebaud et al. 2014). Sibling studies, in which mice are reared to high-fat diets and then switched to control diets until their body weight and fasting glucose level reached that of their control fed siblings, revealed that “dieteted” mice failed to regenerate axonal projections to genetically-defined glomeruli (Thiebaud et al. 2014). Because these mice also did not regain normal odorant discrimination ability, we questioned whether the OSNs that survived following the

induction of DIO, yielded typical activation of olfactory circuits. In this study, we exposed obese mice to a preferred odor ligand for the M72 odorant receptor and quantified immediate-early gene activation (*c-fos*) within the remaining M72-OSN circuits compared with those of off-target glomeruli that are not typically responsive to this M72 odor ligand.

Patterned glomerular activity maps are central to odorant quality coding (Ressler et al. 1994; Vassar et al. 1994; Mombaerts et al. 1996; Takahashi et al. 2004; Murthy 2011; Ma et al. 2012). The glomerulus is comprised of axons of the OSNs, dendrites of the mitral/tufted cells (M/T), and dendrites of the periglomerular (PG) cells. Surrounding the glomeruli are two major types of interneurons, granule and periglomerular cells (Arruda et al. 2013), the latter of which have somata directly circumscribing the glomerulus, hence the traditional derivation of their name – periglomerular cells (Pinching and Powell 1971). Juxtglomerular (JG) lamina, or JG cells, have become the more modern term for cells surrounding the glomerulus, and the lamina has been categorized into three morphologically distinct neuronal classes, periglomerular (PG) cells, superficial short-axon cells (sSA), and external tufted (ET) cells (Nagayama et al. 2014). These neurons play critical roles in synaptic integration and odor processing where they coordinate the activity of the principal excitatory neurons of the olfactory bulb; the mitral cells (Nagayama et al. 2014). The periglomerular cells, which make up the largest percentage of the JG cells, exert their integration of olfactory information by forming reciprocal dendrodendritic synapses with the dendrites of the mitral cells (Pinching and Powell 1971).

In this current study, we examined *c-fos* positive (*c-fos*+) JG cells in M72-IRES-*tau*GFP mice as an indication of OSN circuit activation (Loch et al. 2015) surrounding the odor-stimulated M72 glomerulus following the induction of DIO in mice. In this mouse model, M72-expressing OSNs project their axons to two glomeruli per olfactory bulb, one medially and one laterally. We hypothesized that there should be a concomitant loss in JG cells following DIO given the known loss in glomerular size and OSN abundance (Thiebaud et al. 2014), and that activation of the JG neurons surrounding the stimulated glomerulus, not lost to obesity, would show less immediate-early gene activation. OSNs residing in the nasal septum generally innervate medial glomeruli whereas those residing in the turbinates innervate lateral glomeruli, therefore, we also explored whether these two populations of synaptic targets were differentially sensitive to the effects of DIO.

Materials and methods

Solutions and antibodies

Phosphate-buffered saline (PBS) was prepared as described in Tucker and Fadool (2002). Blocking solution (BS) consisted

of: 0.3% Triton X-100 in PBS containing 2% bovine serum albumin (BSA; Fraction V, #85040C, Sigma Chemical, St. Louis, MO). The odorant molecule, isopropyl tiglate ($C_8H_{14}O_2$; W322903), was purchased from Sigma Chemical. All salts and other reagents were purchased from Sigma Chemical or Fisher Scientific (Atlanta, GA).

c-Fos polyclonal antibody (sc-52-G, Santa Cruz Biotechnology, Dallas, TX) was derived in goat, generated against a peptide targeted to a c-terminal epitope of the human sequence. It was applied at 1:400 in blocking solution as per manufacturer's directions. Specificity controls included Western blot of purified protein (Santa Cruz technical sheet) and application to an array of brain tissues by immunocytochemical methods, for example (Varga et al. 2015) including that of the olfactory bulb by Loch et al. 2015. Polyclonal antisera effective in detergent-solubilized membrane fractions and histological sections for recognizing mMOR28 (Barnea et al. 2004) were a generous gift from Dr. Richard Axel (Columbia University, New York, NY). Later aliquots could be purchased from Fisher Scientific (cat 05R00212W). α -mMOR28 antisera were generated against two unique epitopes, one in the extracellular domain (residues 167–182) and another in the C-terminal tail domain (residues 302–313). These antisera were previously fully characterized by the Axel laboratory (see online supplemental data in Barnea et al. 2004). Specificity controls for α -mMOR28 included complete overlapping patterns with those generated by β -galactosidase staining using MOR28-IRES-tau-LacZ mice. Lack of antibody staining was also confirmed in isolated membrane fractions of adult main olfactory epithelium (MOE) in mice with a gene-targeted deletion of MOR28.

Species-specific secondary antisera in this study were applied at 1:200 in BS and included: Alexa 546 Fluoro donkey anti-goat (A11056; Invitrogen/Thermo Fisher Scientific, Atlanta, GA) and Alexa 647 Fluoro F(ab')₂ Fragment donkey anti-rabbit (711–606-152; Jackson ImmunoResearch Laboratories, Chester County, PA).

Animals and diet

M72-IRES-*tau*GFP mice (agouti background strain) were generated previously via placement of an internal ribosome entry site (IRES) directing the translation of tau:gfp fusion protein immediately downstream from the M72 (Olf1r160) odorant receptor stop codon. These mice were a generous gift from Dr. Peter Mombaerts (Max Plank Institute, Frankfurt, Germany). The M72-IRES-*tau*GFP mice were bred with C57BL6/J (*Mus musculus*, Jackson Laboratories, Bar Harbor, ME) to generate homozygous knockin of the M72 odorant receptor on a mixed agouti/C57BL6/J background. We generated this mixed background in the mice because it was known that C57BL6/J mice were sensitive to dietary-induced changes in olfactory structure, behavioral function,

and biophysical properties of their OB neurons (Fadool et al. 2011; Tucker et al. 2012; Thiebaud et al. 2014). The agouti mutation (*Avy*) can act as an antagonist to the MC4R receptor (Moussa and Claycombe 1999), which we previously studied in MC4R^{-/-} mice as a model of genetic-induced obesity (Tucker et al. 2008; Thiebaud et al. 2014). Following outcrossing, we did not observe this type of *Avy* phenotype (early onset of type II diabetes, hyperphagic, and obese by 2 months of age) in our mixed background mice. All mice were housed in the Florida State University vivarium and were maintained on a 12 h/12 h light-dark cycle and in accordance with institutional requirements for animal care. Mice were individually housed in conventional-style rodent cages containing separate water and food that could be obtained *ad libitum*. Cage design has been reported to affect bulbar development (Oliva et al. 2010). Cage tops were not outfitted with HEPA filtration or individual ventilation (IVC), but room air circulation was standardized at 19 changes/h, and soiled litter was replaced once or twice weekly.

Experiments used male mice that we have previously demonstrated respond to diet-induced obesity (Tucker et al. 2008). Mice were weaned to control or fatty diets at postnatal 23 and maintained on that diet for 6 months. Control food (CF) was comprised of 13.5% kcal fat, 59.81% kcal carbohydrate, and 28.05% kcal protein (Purina 5001 Rodent Chow, St. Louis, MO). Moderately high-fat (MHF) diet was comprised of 31.8% kcal fat, 51.4% kcal carbohydrate, and 16.8% kcal protein (Catalog No. D12266B, Research Diets, New Brunswick, NJ). High-fat (HF) diet was comprised of 60% kcal fat, 20% kcal carbohydrate, and 20% kcal protein (Catalog No. D12492, Research Diets).

Vertebrate animal protocol and anesthesia

All animal procedures were reviewed and approved by FSU Laboratory Animal Resources (Protocols #1427/#1733) that abided by AVMA-approved methods. In preparation for histology, mice were anesthetized by intraperitoneal (i.p.) injection of ketamine (100 mg/kg; Henry Schein Animal Health, Dublin, OH) and xylazine (10 mg/kg; Akorn Animal Health, Lake Forest, IL). This dose of anesthesia was approved as non-survival. The level of anesthesia prior to perfusion was secondarily confirmed by toe pinch and absence of an ocular reflex. Each mouse was intracardially perfused with 1× phosphate-buffered saline (PBS) followed by 4% paraformaldehyde (PFA), prior to decapitation.

Intraperitoneal glucose tolerance test (IPGTT)

Following the 6-month dietary challenge, mice underwent an intraperitoneal glucose tolerance test (IPGTT) to assess their ability to clear glucose. Tail blood sampling from 13 h fasted animals (dark cycle) was used to determine initial fasting

glucose levels using an Ascensia Contour Blood Glucose System (Bayer Healthcare, Whippany, NJ). Clearance of serum glucose over time (10, 20, 30, 60, 90, and 120 min) was then monitored in response to 1 g/ml glucose per kg body weight (University of Virginia Vivarium Protocols, Susanna R. Keller). Glucose tolerance was then determined by integrating the area under the curve (iAUC) as previously (Thiebaud et al. 2014).

Odor exposure

Mice were maintained under “reverse light cycle” so that we could introduce them to the stimulation chamber 2 h following the onset of their dark cycle, or at 0900. Mice were placed in a custom-made stimulation chamber (Fig. 1) (Westberry and Meredith 2003) to present the odor, isopropyl tiglate ($C_8H_{14}O_2$); a preferred ligand that activates the M72 odorant receptor (Soucy et al. 2009; Zhang et al. 2012). The stimulation chamber consisted of a gasket-sealed, glass bell-jar connected to two intake valves that delivered either carbon-cleaned air or odorant-infused air in a cyclic pattern (Zhang et al. 2012). A third exhaust valve allowed for removal of carbon dioxide. A constant flow of air was supplied from a compressed tank (40 psi; medical proof compressed air, Airgas, Tallahassee, FL), which was filtered through a carbon-containing flask prior to being introduced into the chamber as carbon-cleaned air. A second carbon-containing

flask was used to filter the odorant, which was diluted 1:50 in mineral oil (Fisher Scientific). To minimize exposure and spurious *c-fos* activation by ambient odorants, animals were first exposed to carbon-cleaned air for 120 min (min) prior to odorant stimulation. The odor stimulation protocol consisted of 2 min odorant exposure and 5 min of carbon-cleaned air for a total of four cycles (Picospritzer II, Parker Hannifin, Cleveland, OH). Cyclic odor stimulation was used to avoid odor acclimation and desensitization (Zhang et al. 2012). After all cycles were completed, mice remained in the chamber for 60 additional min to optimize immediate-early gene expression prior to sacrifice, as described above.

Immunocytochemistry

Following anesthesia and fix perfusion as above (Ethical statement), mice were decapitated and heads were post-fixed in 4% PFA/PBS for 1 day at 4 °C. Heads were decalcified in 0.3 M EDTA for 48 h at 4 °C. Both the nasal epithelium and olfactory bulbs were removed from the bone and cryoprotected by successive 10 and 30% sucrose in PBS at 4 °C. Tissues were mounted in O.C.T. Compound (Tissue-Tek, Miles Diagnostic Division, Pittsburg, PA), sectioned at 16 μm with a LEICA model CM1850 cryostat (Leica Microsystems, Wetzlar, Germany), and transferred onto plus Superfrost slides (VWR International, Radnor, PA), which were stored at −20 °C until use.

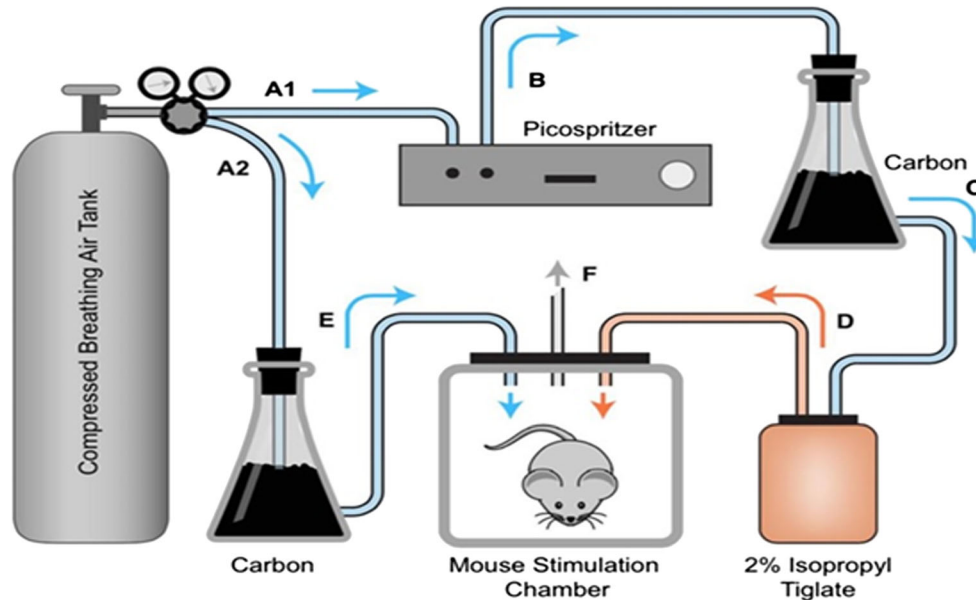


Fig. 1 Schematic of olfactory stimulation of immediate-early genes. Compressed air was alternatively directed (A1 vs. A2) so that mice could be stimulated with 4 rounds of alternating clean air (2 min) and odor-exposed air (5 min) to avoid olfactory desensitization. Clean air was initially delivered to a picospritzer (B) that would drive a 2 min pulse through a carbon-containing flask (C), prior to being passed through an olfactometry bottle containing 10 ml of 2% isopropyl tiglate (D), and then finally introduced to the mouse stimulation chamber (F). The tank was then switched to A2 to allow passage of air through a separate carbon-

containing flask (E) to introduce clean background air to the mouse stimulation chamber for 5 min. Air could be naturally exhausted from the mouse stimulation chamber (4 L Bell Jar) using an output valve (F). To prevent background odors from interfering with *c-fos* baseline stimulation, mice were placed in the stimulation chamber two hours prior to the cyclic delivery of clean/odorized air and received clean air for this duration (A2). Likewise, following the cyclic delivery of clean/odorized air, mice remained in the chamber for one hour to allow *c-fos* expression to plateau prior to sacrifice

Frozen sections were prepared for labelling with c-fos antibody by air drying for 30 min and then rinsing in PBS for 10 min at room temperature (rt). Sections were incubated overnight at 4 °C in the primary antibody diluted in blocking solution, rinsed in PBS to wash unbound antibody, and then incubated for 2 h at rt in species-specific secondary antibody. Secondary antibody was removed by rinsing in PBS and nuclei were stained with 1 µg/mL 4',6-diamidino-2'-phenylindole dihydrochloride (DAPI) (1:15,000; Sigma Chemical) for 10 min at rt. prior to mounting with Fluoromount (Southern Biotech, Birmingham, AL). Sections were viewed and images acquired at 40X magnification using an EVOS FL color system (Model AMF4C3000, Life Science, Calsbad, CA).

Quantitative analysis

Images were imported into Adobe Photoshop CS (San Jose, CA), where image brightness and contrast were adjusted for maximum clarity. Cell counting and glomerular volume measurement was performed according to the quantitative analyses described by Oliva et al. 2008. As such, data from not more than two glomeruli were collected per mouse (one lateral and one medial). Whether the left or right OB was measured for a mouse was randomized. For each mouse, a total of ten, 16 µm sections were tabulated for each lateral or medial glomerulus. Mice that had any missing sections were not used in the analysis (only full section sets were used as experimental mice). The Olfr160 (M72) glomerulus was identified as the green fluorescent protein (GFP)-labelled neuropil. DAPI-stained and c-fos positive immunoreactive juxtglomerular cells (c-fos + JG) were manually counted using ImageJ (<http://imagej.nih.gov/ij/>). Although technological advances have now identified heterogeneity in cell-type identification of many of the neurons in the lamina of the olfactory bulb as recently reviewed (Nagayama et al. 2014), we clustered c-fos + neurons within four cell widths from the glomerulus as our metric for activation of the defined glomerulus, a similar protocol described useful by (Loch et al. 2015). Therefore, no determination of cellular subtype (Bywalez et al. 2017) was attempted on diet-challenged animals given the single goal to quantify and compare immediate-early gene activation of the network associated with the odor-activated, Olfr160 (M72) glomerulus vs. that of off target glomeruli. c-fos + JG cells that belonged to the glomerulus of interest at a maximum of 4 nuclei widths from the glomerular boundary were counted while cells outside this range were excluded (Loch et al. 2015). The percentage of c-fos + JG cells was determined as the fraction of total DAPI-stained cells within the 4-nuclear radii surrounding the glomerulus and was expressed as the mean ± standard error of the mean (SEM).

Data analysis and statistics

Analyses were performed using Origin v8.0 (OriginLab Corporation, Northampton, MA) and GraphPad Prism 6.2 software (San Diego, CA). Data were reported as mean ± SEM. The alpha level for statistical significance was set at 0.05. Normality was determined by the Prism software using the D'Agostino-Pearson omnibus test to measure kurtosis and skewness. The majority of data sets were normally distributed and for these multiple comparison tests, a one-way analysis of variance (ANOVA) using diet as the factor was applied, followed by a Bonferroni *post-hoc* test. Percentage data were not normally distributed and for these multiple comparison tests, a Kruskal-Wallis was applied. IPGTT data were analyzed with a two-way ANOVA using both treatment (diet) and time as factors, followed by a Bonferroni *post-hoc* test.

Results

Induction of DIO

Prior to odorant exposure and mapping of c-fos expression, mice were examined for increased body weight and ability to clear a glucose challenge. A total of 75 male mice were used in all combined experiments of this study. Of the 72 experimental mice, 24 were maintained on control food (CF) diets while 48 were challenged with fatty diets (MHF = 19 mice and HF = 29 mice). Three mice were removed from the study because they developed dermatitis contributed from the fatty oils of the chow. Our studies were limited to male mice. Despite the fact that female mice could afford a good negative control (female mice do not gain a significant amount of weight or adiposity (Tucker et al. 2008)), the 6 month duration of the diet prevented us from including females in our current study. As anticipated from previous studies using IRES-*tau*-LacZ lines (Thiebaud et al. 2014), the M72-IRES-*tau*GFP mice weaned to modified fatty diets gained a significant amount of body weight compared to that of control chow (Fig. 2a; one-way analysis of variance (ANOVA) using body weight as the factor, $p < 0.0001$, Bonferroni's *post-hoc* test). The fasting glucose was not significantly different between control and modified fatty diets, but when presented with a glucose challenge, the ability to clear glucose was significantly impaired for mice maintained on the MHF and HF diets (Fig. 2b; two-way repeated measure ANOVA using time and diet as factors, $p < 0.0001$, Bonferroni's *post-hoc* test). Mice challenged with the HF diet had an elevated plasma glucose level 20 min following the glucose injection whereas those fed a MHF diet were significantly elevated at 30 min ($p < 0.01$). The overall time for clearance of glucose determined through integration of the area under the curve (iAUC) method (Fig. 2b inset) was significantly greater in both the MHF-

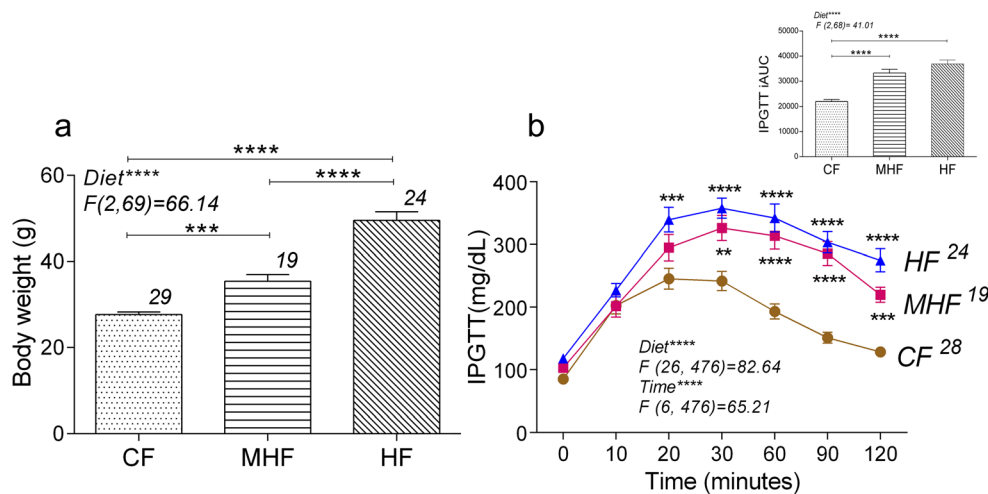


Fig. 2 Change in body weight and glucose clearance in response to maintenance on fatty diets in M72-IRES-*tau*-GFP mice. **a** Bar graph of the mean body weight of mice following maintenance on control food (CF; 13.5% fat, dotted bar), moderately high-fat (MHF; 32% fat; horizontal lined bar), or high-fat (HF; 60% fat, diagonal lined bar) diet from the time of weaning to 6-months of age. Data represent mean \pm standard error of the mean (SEM) with sample sizes as number of mice. **b** Line graph of the concentration of plasma glucose over time following an intraperitoneal glucose tolerance test (IPGTT) for the various 6-month diet treatments. Time 0 = overnight fasting glucose concentration. CF = brown circle, MHF = pink square, HF = blue triangle. Inset, Bar graph of

the integration of the area under the curve (iAUC) vs. dietary treatment. Data represent mean \pm SEM with sample sizes as number of mice. Analyzed factors, F value, degrees of freedom, number of measurements, and *p* value as noted (*****p* < 0.0001, ****p* < 0.001, ***p* < 0.01). One-way analysis of variance (ANOVA) using diet as the factor, *****p* < 0.0001, followed by a Bonferroni's *post-hoc* test (**a**); two-way repeated measure ANOVA using time and diet as factors, *****p* < 0.0001, followed by a Bonferroni's *post-hoc* test (**b**); one-way ANOVA using diet as the factor, *****p* < 0.0001, followed by a Bonferroni's *post-hoc* test (**b**, inset)

and HF-treated mice (one-way ANOVA using diet as the factor, *p* < 0.0001, Bonferroni's *post-hoc* test). These data indicated that the M72-IRES-*tau*GFP mice were an adequate model for pre-diabetes due to the significant increase in body weight and combined decreased efficiency in glucose clearance following induction of DIO.

Abundance of JG cells and glomerular volume in response to DIO

Induction of DIO reduces the cross-sectional size of both the medial and lateral glomerulus (Thiebaud et al. 2014) so we conjectured that there would be a concomitant decrease in the number of associated JG circumscribing each of these glomeruli. We therefore quantified the number of JG cells within a four cell radius of the M72 lateral and medial glomerulus as guided by dapi nuclear stain in association with GFP-labeled glomeruli (Fig. 3). Contrary to our expectation, only the medial, but not the lateral glomerulus, contained a change in the abundance of associated JG cells (Fig. 3a–b; One-way ANOVA, *p* = 0.4136 lateral, *p* = 0.0009 medial). For the medial glomerulus, a Bonferroni's *post-hoc* test indicated that there was an effect for diet where the mice maintained on MHF diet had fewer JG cells associated with the M72 medial glomerulus than did those maintained on CF diet. A similar pattern was observed for JG cells associated with the M72 lateral glomerulus (trended to be fewer), but it did not reach statistical significance.

Odorant activation of c-fos expression in JG cells associated with the M72 glomerulus

OSN activation was mapped following odorant stimulation using *c-fos* labeling (Hu et al. 1994). The immediate-early gene *C-fos* is rapidly and transiently activated in which the strength of the odor or sensory perception could be correlated to the degree of transcription. It would enable a spatial map through which to visualize any altered activity pattern (Schaefer et al. 2002) that might arise upon olfactory stimulation, which was attributed to the DIO state. The level of odor-evoked *c-fos* protein induction in the MOE was not great enough to consistently resolve a signal above clean air basal levels even in CF treated control cohorts (data not shown), therefore we alternatively quantified expression in the olfactory bulb, for which inducible *c-fos* protein levels are known to be adequate for strong antigenicity of the primary antibody (Oliva et al. 2008; Loch et al. 2015). Photomicrographic images were acquired for mice stimulated with clean air only (Fig. 4a) in comparison to those stimulated with isopropyl tiglate (Fig. 4b). For both the lateral and medial M72 glomerulus, there was an effect of odor stimulus (Fig. 4c, d; two-way ANOVA, Tukey's *post-hoc* test with odor stimulation as the factor; lateral *p* = 0.0057; medial *p* = 0.0306) and the *post-hoc* test indicated a significant increase in *c-fos* activation following odor stimulation over that of clean air for animals that were maintained on CF diet (lateral *p* < 0.01; medial *p* < 0.05). Mice that were maintained on MHF or HF diets

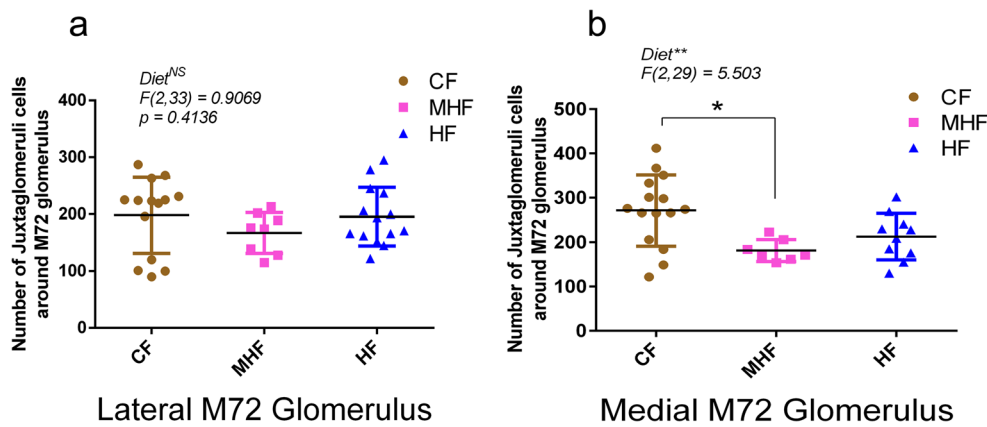


Fig. 3 Reduction in the number of juxtaglomerular cells around the medial M72 glomerulus in response to maintenance on a MHF diet. Box plot of the number of juxtaglomerular cells around the M72 (a) lateral or (b) medial glomerulus. Symbols and dietary treatment as in Fig. 2. Sample size is the number of glomeruli sampled as up to 2 per

mouse. Middle line is the mean \pm SEM. One-way ANOVA using diet as factor, $p = 0.4136$ lateral, NS = not significantly different (a); One-way ANOVA using diet as factor, $**p < 0.01$ medial, followed by a Bonferroni's *post-hoc*, $*p < 0.05$

failed to show an increase in *c-fos* activation following odor stimulation over that of clean air. For the lateral but not the medial M72 glomerulus, there was an effect of diet (Fig. 4c, d; two-way ANOVA, Tukey's *post-hoc* test with diet as the factor; lateral $p = 0.0068$; medial $p = 0.2396$). Mice maintained on fatty diets exhibited a decrease in the percent of *c-fos*-positive JG cells around the M72 lateral glomerulus following odor stimulation compared with that of CF-diet treated animals. The loss was progressive, increasing between the MHF- and HF-diet. When the percent of odor-activated, *c-fos*-positive JG neurons were normalized to the level of activation observed in clean air (Fig. 4e) it was apparent that the JG neurons surrounding the lateral glomerulus exhibited a loss of activity that was diet dependent whereas those surrounding the medial glomerulus were relatively diet insensitive. Collectively these data indicate that diet affects neuronal excitability as determined via immediate-early gene activation of JG cells surrounding the lateral M72 glomerulus when stimulated with its preferred odor ligand.

Discussion

Despite the fact that mice lose olfactory ability and structure when maintained on fatty diets, less is known regarding the function of the remaining glomeruli and correlate neuronal excitability in the obese mouse. Our data indicate that diet-induced obesity, which leads to poor glucose clearance, does not significantly alter the abundance of JG cells surrounding an identified glomerulus. However, neuronal excitability is significantly increased when CF-fed mice are stimulated by a preferred odorant, but is not, if animals are maintained on fatty diets. Odor-stimulated mice are sensitive to increased dietary fat and lose neuronal excitability of interneurons surrounding the lateral but not medial glomerulus.

Lodovichi et al. (2003) explored an intrabulbar circuitry that reciprocally connected isofunctional odor columns on the medial and lateral sides of the olfactory bulb (Lodovichi et al. 2003). They hypothesized that the odor columns functioned for olfactory contrast enhancement via the formation of inhibitory surrounds of the mitral/tufted cells. Our immediate-early gene activation results suggest that there is differential sensitivity to fatty diets across the lateral versus medial glomerulus. OSNs in the nasal septum usually innervate the medial glomeruli, while the OSNs in the turbinates target the lateral glomeruli. Previously we observed a loss of OSNs in response to DIO, but did not distinguish which population of OSNs were projecting to the lateral vs. medial glomerulus only that they were derived from MOR28- or M72-projecting OSNs or were OMP+ (Thiebaud et al. 2014). There may be inherent differences in how these two populations of OSNs respond to DIO. Interestingly, Restrepo and colleagues noted that the 'two mirror image' glomerular maps for the P2 glomeruli demonstrated neuroanatomical and functional asymmetry (Oliva et al. 2008). The JG neurons surrounding the lateral glomerulus had a higher proportion of tyrosine hydroxylase labeling than those surrounding the medial glomerulus and had higher responsivity to volatile odorants. They found that the lateral glomerulus had greater *c-fos* activation in response to odorant stimulation (urine) than that of the medial glomerulus. If the dual map in olfaction allows contrasting differential input as an additional source of coding information to the olfactory bulb (Lodovichi et al. 2003), then DIO could bring an imbalance with the loss of sensitivity of the lateral glomerulus. It is also known that intrabulbar connections can modulate mitral/tufted cell receptive fields and that JG cells receive input from these neurons. DIO dampens the excitability of mitral/tufted cells and their sensitivity to neuromodulation (Fadool et al. 2011) so it would not be surprising that JG cells exhibited a reduced *c-fos* activation. Why

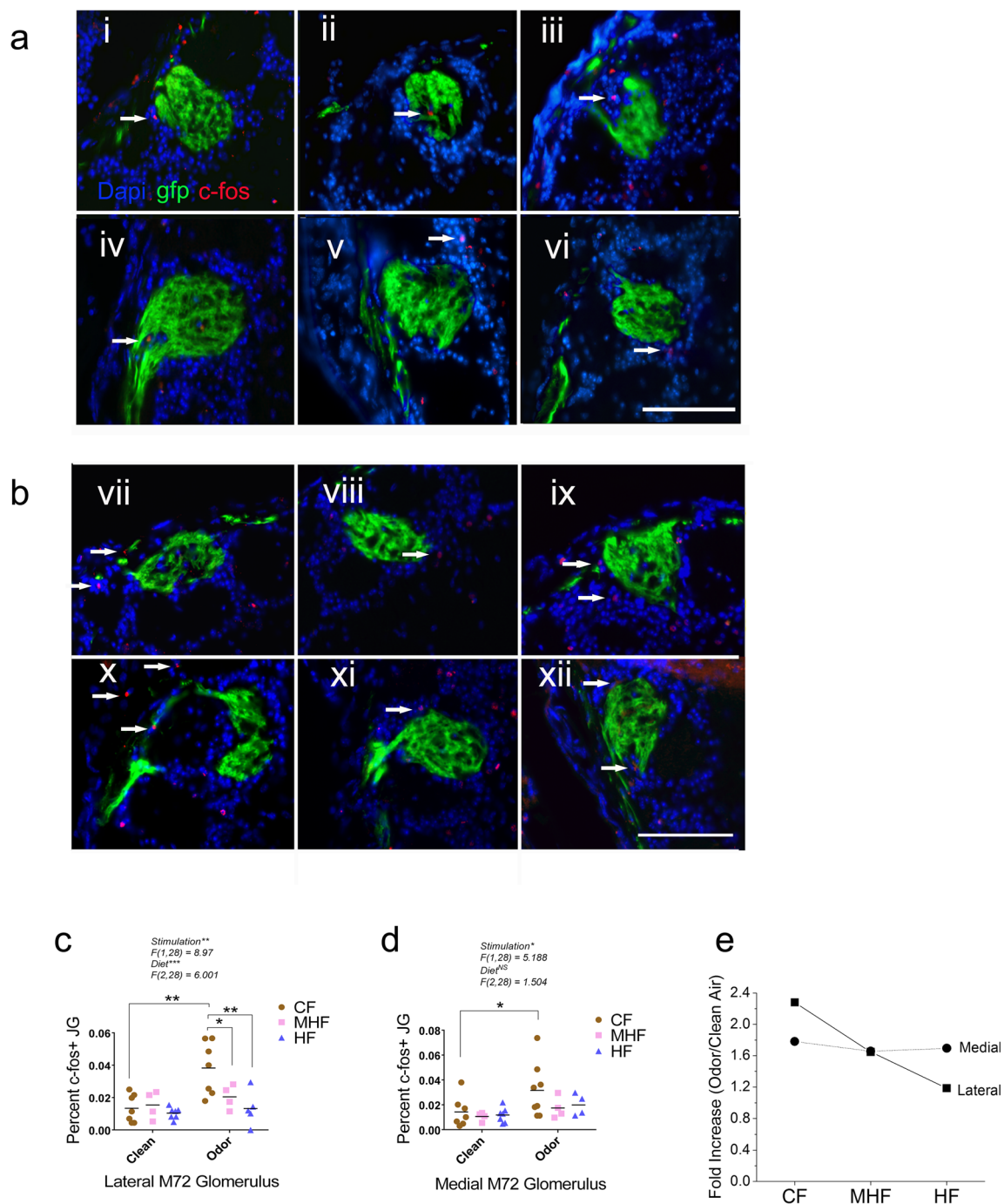


Fig. 4 Odor-evoked *c-fos* activation in the juxtglomerular cells surrounding the lateral but not the medial M72 glomerulus in *M72-IRES-tau-GFP* mice. Photomicroscopic images of the M72 glomerulus in *M72-IRES-tau-GFP* mice (*gfp*; green) surrounded by their associated juxtglomerular cells (*dapi* nuclear stain; blue), some of which demonstrate *c-fos* immediate-early gene activation (arrows; red) in response to **(a)** clean-air stimulation or **(b)** isopropyl tiglate stimulation. Top rows, or i – iii and vii – ix = lateral glomeruli. Bottom rows, or iv – vi and x–xii = medial glomeruli. Left column, or i, iv, vii, and x = CF. Middle column, or ii, v, viii, and xi = MHF. Right column, or iii, vi, ix, and xii = HF. Plot of the percentage of *c-fos* positive (+) juxtglomerular cells (JC)

surrounding the M72 **(c)** lateral vs. **(d)** medial glomerulus. Line = mean with sample size as a M72 glomerulus quantified as per *c-fos* activation per mouse. **e** Line graph of the fold increase in mean *c-fos* activity for JG cells of the M72 medial vs. lateral glomerulus comparing odor/clean air stimulation conditions for the data presented in **(c)** and **(d)**. Symbols and statistical notations as in Fig. 2. Two-way analysis of variance (ANOVA) using diet and odor stimulation as factors followed by a Bonferroni's *post-hoc* test, $**p < 0.01$, $***p < 0.001$ **(a)**; Two-way analysis of variance (ANOVA) using diet and odor stimulation as factors followed by a Bonferroni's *post-hoc* test, $*p < 0.05$, NS = not significantly different **(b)**

it was specifically lateral vs. medial, however, is not understood. It has been suggested that mirror image, symmetrical activation of glomerular maps is more consistently found through stimulation with single odorant molecules as opposed to that of complex odorants or mixtures (Schaefer et al. 2002; Xu et al. 2000). It would be interesting in this regard to systematically examine how DIO might disrupt varying odorant qualities, especially given the chromatographic nature of the epithelium (Mozell 1970).

There is a linear correlation between the number of OSNs expressing a defined OR gene and the volume of the targeted olfactory glomerulus (Bressel et al. 2016). Mombaerts and colleagues derived a linear correlation for 15 OR-IRES-designed mice strains (including M72IRES*tau*GFP) so that volume of the glomerulus could be a surrogate for the number of OSNs sending genetically-identified axonal projections to that glomerulus. Because we know that DIO causes a loss of OSNs and a concomitant loss of glomerular cross-sectional area (Thiebaud et al. 2014), we were surprised to find no change in JG abundance surrounding the M72-glomerulus. Reduced-sized glomeruli following DIO, would have to support an increased density of JG cells in order for there not to be a change in abundance around the smaller structure in mice maintained on the fatty diets. Loss of OSNs attributed to DIO may thereby be resculpting the olfactory bulb as a compensatory mechanism. This idea of normalization was recently brought forth by Roland et al. 2016 who suggest a means by which a substantially degraded odor input (in our case, loss of OSNs) can still be transformed for meaningful OB output. This would be consistent with our finding that mice made obese through fatty diet have a decreased odorant discrimination but are able to detect odors (Tucker et al. 2012; Thiebaud et al. 2014). If our observed decrease in number of c-fos-activated JCs was correlated to the reduction in OSNs following a MHF challenge (Thiebaud et al. 2014), then it could be extrapolated that fatty diets could additionally impact the intrinsic excitability of other neuronal populations in the olfactory system. In previous studies, we found that mitral cells exhibited a change in basal AP firing frequency and decreased sensitivity to insulin after the mice were challenged with a MHF diet (Fadool et al. 2011). In other brain areas, such as the hippocampus or the hypothalamus, it has been demonstrated that fat-enriched diets elicit a significant reduction in neuronal excitability (Pancani et al. 2013; Underwood and Lucien 2016; Paeger et al. 2017). For example, pro-opiomelanocortin (POMC)-expressing neurons in the arcuate nucleus of the hypothalamus have been found to have a drastic reduction in spontaneous spiking activity and an increased spike adaptation in mice fed with high-fat diets (Paeger et al. 2017). The modifications in spiking properties of POMC-neurons have been linked to the alteration in intracellular Ca^{2+} handling properties. Interestingly, in the same animals, a decrease in mitochondrial Ca^{2+} stores of POMC-neurons was reported.

These observations are in line with a recent study from our laboratory showing an alteration of the morphology of mitochondria in the olfactory bulb following MHF diet in mice (Kovach et al. 2016). Such alteration could lead to a modification of the intrinsic excitability of the neurons in the olfactory bulb given the high requirement of energy known to support AP firing (Nawroth et al. 2007).

There are a number of computational models and experimental reports that try to define the physiological role of inhibitory circuits in controlling mitral cell spiking, as the principle output neuron of the olfactory bulb (Cleland and Linster 2005; Arevian et al. 2008; Cleland and Linster 2012; Arruda et al. 2013). Not only are there morphologically distinct subclasses of JG cells forming these inhibitory circuits – PG cells, ET cells and sSA cells (Nagayama et al. 2014), there is also further heterogeneity within the subclasses. Our study did not incorporate a distinction across JG cells, only quantifying immediate early-gene activity within a 4-cell thick location around the circumference of the glomerulus. The most numerous JG cells are GABAergic periglomerular cells or PGCs (Parrish-Aungst et al. 2007) that largely project their dendrites into one, or at most, two glomeruli, yet another large subgroup are both dopaminergic and GABAergic (named JGCs) and have innervation that is multiglomerular in nature (Kiyokage et al. 2010). There is also a difficult distinction between juxtglomerular and intraglomerular neuropil or ‘shells’ first noted by Pinching and Powell (1971), nonetheless we attempted to make our quantifications standard regardless of dietary treatment. Future experiments could seek subtype identification of the c-fos positive neurons as greater functional and anatomical distinctions between JG cells are refined, for example, see Bywalez et al. (2017). A final interpretation is that c-fos activation could be induced in astrocytes that surround the glomerulus, which have recently been reported to have an expansion of their processes in response to fasting (Daumas-Meyer et al. 2018). Although our studies did not employ fasting, rather a modified diet, further study would be required to determine if such a diet-induced astrocytic mechanism were at play. C-fos activation of astrocytes via glutamate signaling is not well understood, can result from by proliferation or development rather than depolarization, and novel routes of activation have been reported (Hisanaga et al. 1994; Edling et al. 2007; Adamsky et al. 2018).

In conclusion, we have demonstrated that DIO causes deleterious effects on OSN survival that extends to a reduced neuronal activity of JG cells surrounding the genetically-identified glomerulus for that class of ORs. In the process, we have identified an asymmetry in the responsiveness of the ‘mirror image’ glomerular map for the M72 receptor that shows greater sensitivity of the lateral vs. medial glomerulus towards fatty diets.

Acknowledgements We would like to thank Mr. William Speranza, Ms. Abigail Thomas, and Mr. W. Joshua Earl for husbandry of our mouse colonies, maintenance of modified diets, and routine technical assistance. We would like to thank Dr. Thomas G. Mast for helpful suggestions in the analysis. We would like to thank Dr. Michael Meredith for design of the odor stimulation chamber and Mr. Charles Badland for artwork in Fig. 1. This work was supported by National Institutes of Health (NIH) T32 DC000044 and R01 DC013080 from the National Institutes of Deafness and Communication Disorders (NIDCD) and a Phi Eta Sigma Florida State University (FSU) Undergraduate Research Award.

Compliance with ethical standards

Ethical approval All applicable international, national, and/or institutional guidelines for the care and use of animals were followed. All procedures performed in studies involving animals were in accordance with the ethical standards of the institution or practice at which the studies were conducted.

Conflict of interest The authors declare that they have no conflict of interest.

References

- Adamsky A, Kol A, Kreisel T, Doron A, Ozeri-Engelhard N, Melcer T, Refaeli R, Horn H, Regev L, Groysman M, London M, Goshen I (2018) Astrocytic activation generates de novo neuronal potentiation and memory enhancement. *Cell* 174(1):59–71. <https://doi.org/10.1016/j.cell.2018.05.002>
- Arevian AC, Kapoor V, Urban NN (2008) Activity-dependent gating of lateral inhibition in the mouse olfactory bulb. *Nat Neurosci* 11:80–87. <https://doi.org/10.1038/nn2030>
- Arruda D, Publio R, Roque AC (2013) The periglomerular cell of the olfactory bulb and its role in controlling mitral cell spiking: a computational model. *PLoS One* 8:e56148. <https://doi.org/10.1371/journal.pone.0056148>
- Barnea G, O'Donnell S, Mancia F, Sun X, Nemes A, Mendelsohn M, Axel R (2004) Odorant receptors on axon termini in the brain. *Science* 304:1468. <https://doi.org/10.1126/science.1096146>
- Bressel OC, Khan M, Mombaerts P (2016) Linear correlation between the number of olfactory sensory neurons expressing a given mouse odorant receptor gene and the total volume of the corresponding glomeruli in the olfactory bulb. *J Comp Neurol* 524:199–209. <https://doi.org/10.1002/cne.23835>
- Bruce-Keller AJ, Keller JN, Morrison CD (2009) Obesity and vulnerability of the CNS. *Biochim Biophys Acta* 1792(5):395–400. <https://doi.org/10.1016/j.bbadis.2008.10.004>
- Bywalez WG, Ona-Jodar T, Lukas M, Ninkovic J, Egger V (2017) Dendritic arborization patterns of small juxtglomerular cell subtypes within the rodent olfactory bulb. *Front Neuroanat* 10:127. <https://doi.org/10.3389/fnana.2016.00127>
- Cleland TA, Linster C (2005) Computation in the olfactory system. *Chem Senses* 30:801–813. <https://doi.org/10.1093/chemse/bji072>
- Cleland TA, Linster C (2012) On-center/inhibitory-surround decorrelation via intraglomerular inhibition in the olfactory bulb glomerular layer. *Front Integr Neurosci* 6:5. <https://doi.org/10.3389/fnint.2012.00005>
- Daumas-Meyer V, Champeil-Potokar G, Chaumontet C, Dahirel P, Papillon C, Congar P, Denis I (2018) Fasting induces astroglial plasticity in the olfactory bulb glomeruli of rats. *Glia* 66(4):762–776. <https://doi.org/10.1002/glia.23280>
- Edling Y, Ingelman-Sundberg M, Simi A (2007) Glutamate activates c-fos in glial cells via a novel mechanism involving the glutamate receptor subtype mGlu5 and the transcriptional repressor DREAM. *Glia* 55(3):328–340. <https://doi.org/10.1002/glia.20464>
- Fadool DA, Tucker K, Pedarzani P (2011) Mitral cells of the olfactory bulb perform metabolic sensing and are disrupted by obesity at the level of the Kv1.3 ion channel. *PLoS One* 6:e24921. <https://doi.org/10.1371/journal.pone.0024921>
- Hisanaga K, Sagar SM, Hicks KJ, Swanson RA, Sharp FR (1994) c-fos proto-oncogene expression in astrocytes associated with differentiation or proliferation by not depolarization. *Brain Res Mol Brain Res* 8(1):69–75
- Hu E, Mueller E, Oliviero S, Papaioannou VE, Johnson R, Spiegelman BM (1994) Targeted disruption of the c-fos gene demonstrates c-fos-dependent and -independent pathways for gene expression stimulated by growth factors or oncogenes. *EMBO J* 13:3094–3103
- Kiyokage E, Pan YZ, Shao Z, Kobayashi K, Szabo G, Yanagawa Y, Obata K, Okano H, Toida K, Puche AC, Shipley MT (2010) Molecular identity of periglomerular and short axon cells. *J Neurosci* 30:1185–1196. <https://doi.org/10.1523/JNEUROSCI.3497-09.2010>
- Kovach C, Al Korbosy D, Huang Z, Chelette BM, Fadool JM, Fadool DA (2016) Mitochondria ultrastructure and glucose signaling pathways attributed to the Kv1.3 ion channel. *Front Physiol* 19(7):178. <https://doi.org/10.3389/fphys.2016.00178>
- Loch D, Breer H, Strotmann J (2015) Endocrine modulation of olfactory responsiveness: effects of the orexigenic hormone ghrelin. *Chem Senses* 40:469–479. <https://doi.org/10.1093/chemse/bjv028>
- Lodovichi C, Belluscio L, Katz LC (2003) Functional topography of connections linking mirror-symmetric maps in the mouse olfactory bulb. *Neuron* 38:265–276
- Ma L, Qiu Q, Gradwohl S, Scott A, Yu EQ, Alexander R, Wiegraebe W, Yu CR (2012) Distributed representation of chemical features and tonotopic organization of glomeruli in the mouse olfactory bulb. *Proc Natl Acad Sci U S A* 109:5481–5486. <https://doi.org/10.1073/pnas.1117491109>
- Mombaerts P, Wang F, Dulac C, Chao SK, Nemes A, Mendelsohn M, Edmondson J, Axel R (1996) Visualizing an olfactory sensory map. *Cell* 87:675–686
- Moussa MN, Claycombe KJ (1999) The yellow mouse obesity syndrome and mechanisms of agouti-induced obesity. *Obes Res* 7(5):506–514
- Moyer VA (2012) Screening for and management of obesity in adults: U.S. preventive services task force recommendation statement. *Ann Intern Med* 157:373–378. <https://doi.org/10.7326/0003-4819-157-5-201209040-00475>
- Mozell MM (1970) Evidence for a chromatographic model of olfaction. *J Gen Physiol* 56:46–63
- Murthy VN (2011) Olfactory maps in the brain. *Annu Rev Neurosci* 34:233–258. <https://doi.org/10.1146/annurev-neuro-061010-113738>
- Nagayama S, Homma R, Imamura F (2014) Neuronal organization of olfactory bulb circuits. *Front Neural Circuits* 8:98. <https://doi.org/10.3389/fncir.2014.00098>
- Nawroth JC, Greer CA, Chen WR, Laughlin SB, Shepherd GM (2007) An energy budget for the olfactory glomerulus. *J Neurosci* 27(36):9790–9800. <http://www.jneurosci.org/content/27/36/9790>
- Ogden CL, Carroll MD, Kit BK, Flegal KM (2014) Prevalence of childhood and adult obesity in the United States, 2011–2012. *JAMA* 311:806–814. <https://doi.org/10.1001/jama.2014.732>
- Oliva AM, Jones KR, Restrepo D (2008) Sensory-dependent asymmetry for a urine-responsive olfactory bulb glomerulus. *J Comp Neurol* 510:475–483. <https://doi.org/10.1002/cne.21800>
- Oliva AM, Salcedo E, Hellier JL, Ly X, Koka K, Tollin DJ, Restrepo D (2010) Toward a mouse neuroethology in the laboratory environment. *PLoS One* 5:e11359. <https://doi.org/10.1371/journal.pone.0011359>

- Paeger L, Pippow A, Hess S, Paehler M, Klein AC, Husch A, Pouzat C, Bruning JC, Kloppenburg P (2017) Energy imbalance alters Ca^{2+} handling and excitability of POMC neurons. *Elife* 1(6):e25641. <https://doi.org/10.7554/eLife.25641>
- Palouzier-Paulignan B, Lacroix MC, Aime P, Baly C, Caillol M, Congar P, Julliard AK, Tucker K, Fadool DA (2012) Olfaction under metabolic influences. *Chem Senses* 37:769–797. <https://doi.org/10.1093/chemse/bjs059>
- Pancani T, Anderson KL, Brewer LD, Kadish I, DeMoll C, Landfield PW, Blalock EM, Porter NM, Thibault O (2013) Effect of high-fat diet on metabolic indices, cognition, and neuronal physiology in aging F344 rat. *Neurobiol Aging* 34:1977–1987. <https://doi.org/10.1016/j.neurobiolaging.2013.02.019>
- Parrish-Aungst S, Shipley MT, Erdelyi F, Szabo G, Puche AC (2007) Quantitative analysis of neuronal diversity in the mouse olfactory bulb. *J Comp Neurol* 501:825–836. <https://doi.org/10.1002/cne.21205>
- Pinching AJ, Powell TP (1971) The neuropil of the periglomerular region of the olfactory bulb. *J Cell Sci* 9:379–409
- Ressler KJ, Sullivan SL, Buck LB (1994) Information coding in the olfactory system: evidence for a stereotyped and highly organized epitope map in the olfactory bulb. *Cell* 79:1245–1255
- Roland B, Jordan R, Sosulski DL, Diodato A, Fukunaga I, Wickersham I, Franks KM, Schaefer AT, Fleischmann A (2016) Massive normalization of olfactory bulb output in mice with a 'monoclonal nose'. *Elife* 13(5):e16335. <https://doi.org/10.7554/eLife.16335>
- Schaefer ML, Yamazaki K, Osada K, Restrepo D, Beauchamp GK (2002) Olfactory fingerprints for major histocompatibility complex-determined body odors II: relationship among odor maps, genetics, odor composition, and behavior. *J Neurosci* 22:9513–9521
- Soucy ER, Albeanu DF, Fantana AL, Murthy VN, Meister M (2009) Precision and diversity in an odor map on the olfactory bulb. *Nat Neurosci* 12:210–220. <https://doi.org/10.1038/nn.2262>
- Takahashi YK, Kurosaki M, Hirono S, Mori K (2004) Topographic representation of odorant molecular features in the rat olfactory bulb. *J Neurophysiol* 92:2413–2427. <https://doi.org/10.1152/jn.00236.2004>
- Thiebaud N, Johnson MC, Butler JL, Bell GA, Ferguson KL, Fadool AR, Fadool JC, Gale AM, Gale DS, Fadool DA (2014) Hyperlipidemic diet causes loss of olfactory sensory neurons, reduces olfactory discrimination, and disrupts odor-reversal learning. *J Neurosci* 34:6970–6984. <https://doi.org/10.1523/JNEUROSCI.3366-13.2014>
- Tucker K, Fadool DA (2002) Neurotrophin modulation of voltage-gated potassium channels in rat through TrkB receptors is time and sensory experience dependent. *J Physiol* 542(2):413–429
- Tucker K, Overton JM, Fadool DA (2008) Kv1.3 gene-targeted deletion alters longevity and reduces adiposity by increasing locomotion and metabolism in melanocortin-4 receptor-null mice. *Int J Obes* 32:1222–1232. <https://doi.org/10.1111/j.1365-2826.2012.02314.x>
- Tucker KR, Godbey SJ, Thiebaud N, Fadool DA (2012) Olfactory ability and object memory in three mouse models of varying body weight, metabolic hormones, and adiposity. *Physiol Behav* 107:424–432. <https://doi.org/10.1016/j.physbeh.2012.09.007>
- Tucker K, Cho S, Thiebaud N, Henderson MX, Fadool DA (2013) Glucose sensitivity of mouse olfactory bulb neurons is conveyed by a voltage-gated potassium channel. *J Physiol* 591:2541–2561. <https://doi.org/10.1113/jphysiol.2013.254086>
- Underwood EL, Lucien T (2016) High-fat diet impairs spatial memory and hippocampal intrinsic excitability and sex-dependently alters circulating insulin and hippocampal insulin sensitivity. *Biol Sex Differ* 28(7):9. <https://doi.org/10.1186/s13293-016-0060-3>
- Varga D, Heredi J, Kanvasi Z, Ruszka M, Kis Z, Ono E, Iwamori N, Iwamori T, Takakuwa H, Vecsei L, Toldi J, Gellert L (2015) Systemic L-Kynurenine sulfate administration disrupts object recognition memory, alters open field behavior and decreases c-Fos immunopositivity in C57Bl/6 mice. *Front Behav Neurosci* 9:157. <https://doi.org/10.3389/fnbeh.2015.00157>
- Vassar R, Chao SK, Sitcheran R, Nunez JM, Vosshall LB, Axel R (1994) Topographic organization of sensory projections to the olfactory bulb. *Cell* 79:981–991
- Westberry JM, Meredith M (2003) Pre-exposure to female chemosignals or intracerebral GnRH restores mating behavior in naive male hamsters with vomeronasal organ lesions. *Chem Senses* 28:191–196
- Xu F, Greer CA, Shepherd GM (2000) Odor maps in the olfactory bulb. *J Comp Neurol* 422:489–495
- Yeomans MR (2006) Olfactory influences on appetite and satiety in humans. *Physiol Behav* 89:10–14. <https://doi.org/10.1016/j.physbeh.2006.04.010>
- Zhang J, Huang G, Dewan A, Feinstein P, Bozza T (2012) Uncoupling stimulus specificity and glomerular position in the mouse olfactory system. *Mol Cell Neurosci* 51:79–88. <https://doi.org/10.1016/j.mcn.2012.08.006>